Research Square

Preprints are preliminary reports that have not undergone peer review.
They should not be considered conclusive, used to inform clinical practice,
or referenced by the media as validated information.

Seismic linear noise attenuation based on the lateral random reorder

Yaoguang Sun

sunyg_guang@126.com

Chengdu North Petroleum Exploration and Development Technology Company Limited
https://orcid.org/0000-0002-8922-2069

Zhipeng Huan

China University of Petroleum East China

Zhou Xie

China University of Petroleum (Beijing)

Jianxiang Feng

China University of Petroleum Beijing

Yingchang Cao

China University of Petroleum East China

Siyuan Cao

China University of Petroleum Beijing

Research Article

Keywords: linear noise, signal-noise difference, rotating coordinate, lateral random reorder

Posted Date: November 6th, 2026

DOI: https://doi.org/10.21203/rs.3.rs-7985162/v2

License: This work is licensed under a Creative Commons Attribution 4.0 International License.
Read Full License

Additional Declarations: The authors declare no competing interests.

Seismic linear noise attenuation based on the lateral random reorder

Yaoguang Sun[1*], Zhipeng Huan[2], Zhou Xie[3], Jianxiang Feng[3], Yingchang Cao[2], Siyuan Cao[3]

1. Chengdu North Petroleum Exploration and Development Technology Company Limited, Chengdu, China, 610213.

2. China University of Petroleum (East China), Qingdao, China, 266580.

3. China University of Petroleum (Beijing), Beijing, China, 102249.

Abstract

Attenuating linear noise remains one of the most persistent challenges in seismic exploration, especially when the target noise is weak in amplitude. Conventional methods usually separate the desired reflections from such noise according to differences in frequency content or apparent velocity. However, these approaches fail when the two components are not sufficiently distinct in those domains, making reliable separation difficult in practice. To overcome this difficulty, we propose a lateral random permutation strategy. The data are first rotated so that the linear events are flattened, and the samples at each time instant are then reordered randomly along the lateral direction. Owing to this shuffling, events whose apparent velocity differs from that of the target noise are broken up and behave as random outliers, which considerably widens the gap between the linear noise and the remaining signal components. Tests on both synthetic and field data confirm, visually and quantitatively, that the proposed method suppresses linear noise effectively while keeping signal loss to a minimum.

Keywords: linear noise, signal-noise separation, rotating coordinate, lateral random reorder

Introduction

For decades, contamination by linear noise has been regarded as one of the most troublesome obstacles in seismic data processing and imaging (Verschuur et al., 1992; Yilmaz, 2001), as it often degrades the continuity of the data and, consequently, the quality of the subsurface image (Wang, 2003; Gan and Peng, 2004). Over the years, a large body of algorithms has been developed to suppress both linear and quasi-linear noise. Methodologically, these conventional techniques fall roughly into two categories: filtering-based approaches and wavefield transformation-based strategies.

Filtering-based methods first map the seismic data into a domain in which signal and noise are more easily separated, and then apply purpose-built filtering operators. As early as 1967, Treitel and colleagues put forward frequency–wavenumber (FK) filtering, which exploits the disparity between the frequency and wavenumber

distributions of signal and noise to remove linear interference. Turner (1990) subsequently resorted to the Radon transform to eliminate spatially aliased linear coherent noise. In a later development, Henley (2003) constructed a coherent-noise removal scheme on the basis of the radial trace transform, attenuating the noise effectively while retaining the fine-scale lateral features of the reflections. Around the same time, Gao et al. (2003) designed an adaptive coherent-noise suppression algorithm that works directly in the time–space domain and proved effective at removing linear noise from seismic sections. Liao et al. (2007) pushed this line of research forward by introducing a three-dimensional differential-equation filtering method inspired by the Butterworth filter. Bekara and Mirko (2009) introduced a strategy that applies empirical mode decomposition (EMD) to frequency slices in the frequency–offset domain and rejects the first intrinsic mode function so as to suppress coherent noise. Liu et al. (2011a) developed an NMO-corrected filtering scheme in the time–offset (T–X) domain that flattens curved coherent noise and then removes it according to differences in apparent velocity. More recently, Tian et al. (2013) combined Fourier-transform filtering with three-dimensional cone filtering on cross-spread acquisition geometries to reduce wide-azimuth linear interference. In the same year, Lu and Li devised a hybrid Radon transform with a similarity function that alleviates endpoint and truncation artifacts, allowing linear noise to be extracted from seismic profiles in a single step.

The second family consists of wavefield transformation-based approaches, which share a common pipeline: the linear noise events are first flattened, the target noise is then fitted with a suitable mathematical transformation, and the estimated noise is finally reconstructed through the corresponding inverse transform and subtracted from the original records. Yedlin et al. (1987) were the first to employ the Karhunen–Loève transform for isolating and enhancing acoustic diffraction signals embedded in background reflections. Lu et al. (2006a) proposed a local polynomial approximation algorithm aimed specifically at locally linear coherent noise; in a companion study, the same group later presented an adaptive singular value decomposition (SVD) method (Lu, 2006b) that enhances non-horizontal events, together with a rotation of the data that aligns the estimated dips horizontally. Liu et al. (2011b) mapped seismic data into the time–apparent velocity domain via the radial trace transform and estimated the linear coherent noise there by means of non-stationary polynomial fitting. Huang et al. (2017) explored mathematical morphological filtering (MMF) for linear noise suppression, exploiting the differences in morphological shape between the useful reflections and the coherent noise along the spatial axis. Inspired by multi-source

deblending, Chen et al. (2021) devised the rotate-time-shift FK transform by formulating random time-shift operators, which further improved the accuracy of linear noise extraction. Beyond these classical frameworks, the rapid progress of deep neural networks has opened up new possibilities for data-driven suppression of linear noise (Yuan et al., 2022), although such approaches are data-hungry and generally depend on large-scale annotated training datasets to achieve satisfactory generalization.

Despite these advances, attenuating weak linear noise that is insufficiently distinct from the reflections in frequency or apparent velocity remains difficult. The main contributions of this work are as follows. First, we propose a lateral random reorder strategy for linear noise attenuation. The data are first rotated so that the linear events are flattened, and the traces are then randomly permuted at each time instant. Under this permutation, reflection events whose apparent velocity differs from that of the target noise lose their lateral coherence and behave as random, outlier-like components, whereas the flattened linear noise remains continuous and its energy stays concentrated near zero wavenumber in the FK domain. The gap between the linear noise and the remaining signal is thereby considerably widened, which is the key to attenuating weak linear noise that cannot be separated on the basis of frequency content or apparent velocity alone. Second, we formulate the extraction of the linear noise as an outlier-attenuation problem and solve it under the "Lp+Lp" framework using the alternating direction method of multipliers (ADMM), with generalized iterative soft-thresholding and shaping-regularization updates. Third, we validate the proposed method on two synthetic models, a noise-robustness study, and a field common-shot gather, and compare it with FK filtering and Radon-domain filtering in terms of both noise suppression and signal preservation. The remainder of this paper is organized as follows. The Method section describes the rotation-flattening and lateral reorder operators and the "Lp+Lp" outlier-attenuation algorithm. The Applications section validates the method on synthetic and field data. The Conclusions and Discussions sections summarize the work and outline its limitations and possible extensions.

Method

1. Data rotation and reorder theory

Assume that $\mathbf{S}_0(x_0, y_0) \in \mathbb{R}^{m_0 \times n_0}$ is the original data containing linear noise and that $\mathbf{S}$ is a subset of $\mathbf{S}_0$, where $\{\mathbf{S}(x,y) | \mathbf{S} \in \mathbb{R}^{m \times n}, m \leqslant m_0, n \leqslant n_0\}$ ($\mathbf{S}$ contains the linear noise, and the more accurate $\mathbf{S}$ is, the more effective the noise suppression becomes). The rotation-flattening operator $\mathcal{L}$ rotates the data as a whole so that the

linear noise is aligned horizontally, while the relative positions between the linear noise and the remaining seismic events are preserved. The rotation-flattening operator $\mathcal{L}$ defines a mapping, which can be expressed as:

$$\begin{aligned} \mathcal{L}(\mathbf{S}(x,y)) &\mapsto \mathbf{S}'(x',y') \\ \mathcal{L}^{-1}(\mathbf{S}'(x',y')) &\mapsto \mathbf{S}(x,y) \end{aligned} \tag{1}$$

Assuming that the linear noise $\mathbf{S}$ has a stable apparent velocity v_a, its dip angle can be computed as $\theta = \arctan(1/v_a)$. Correspondingly, the dimensions of the rotated data can be transformed as:

$$\begin{aligned} n' &= |\cos(\theta)|n + |\sin(\theta)|m \\ m' &= |\cos(\theta)|m + |\sin(\theta)|n \end{aligned} \tag{2}$$

The corresponding rotated coordinates can be constructed as follows:

$$\begin{aligned} x' &= x\cos(\theta) + y\sin(\theta) - \frac{1}{2}n'\cos(\theta) - \frac{1}{2}m'\sin(\theta) + \frac{1}{2}n \\ y' &= y\cos(\theta) - x\sin(\theta) + \frac{1}{2}n'\sin(\theta) - \frac{1}{2}m'\cos(\theta) + \frac{1}{2}m \end{aligned} \tag{3}$$

For the inverse rotation, θ can be replaced with $-\theta$ to restore the original coordinates:

$$\begin{aligned} x &= x'\cos(-\theta) + y'\sin(-\theta) - \frac{1}{2}n\cos(-\theta) - \frac{1}{2}m\sin(-\theta) + \frac{1}{2}n' \\ y &= y'\cos(-\theta) - x'\sin(-\theta) + \frac{1}{2}n\sin(-\theta) - \frac{1}{2}m\cos(-\theta) + \frac{1}{2}m' \end{aligned} \tag{4}$$

For the rotation-flattening operator $\mathcal{L}$, a pair of forward and inverse transforms is obtained, as shown in equations (3) and (4). After rotation-flattening, a sparsity-promoting transform is applied to further scatter the energy of non-horizontal events. The forward and inverse lateral reorder operators are defined as $\mathcal{P}$ and $\mathcal{P}^{-1}$:

$$\mathcal{P}(\mathbf{S}_i) \mapsto \mathbf{S}_{index},\ \mathcal{P}^{-1}(\mathbf{S}_{index}) \mapsto \mathbf{S}_i \tag{5}$$

where $\mathbf{S}_{index}$ denotes the reordered data, and the subscripts i and $index$ define a mapping relationship: i is the i-th trace, and $index$ is the new index of the i-th trace after random sorting. This reorder operator can be applied to the entire dataset globally or separately at each time point:

$$\mathcal{P}(\mathbf{S}_{j,i_j}) \mapsto \mathbf{S}_{j,index_j},\ \mathcal{P}^{-1}(\mathbf{S}_{j,index_j}) \mapsto \mathbf{S}_{j,i_j} \tag{6}$$

where $j(1, 2, 3 \cdots m')$ denotes the j-th time point, while subscripts i_j and $index_j$ represent a mapping relationship at j-th time point: i_j refers to the i-th trace at the j-th time point, and $index_j$ indicates the randomly permuted index of that trace after reorder at time j. $index_j$ corresponds to the new position of trace i_j after random shuffling applied individually at the j-th time point. Global lateral random reorder and multi-time-point lateral random reorder produce different effects. The purpose and outcome of these two reorder strategies are illustrated in detail in Figure 1. Figures 1(a) and (b) show the original data and its FK spectrum, containing three effective signal events and two linear noise components $\mathbf{S}_1$ and $\mathbf{S}_2$. After rotation-flattening (Figures 1(c) and (d)), the linear noise $\mathbf{S}_1$ becomes horizontally aligned. Assuming $\mathbf{S}_1$ is the target linear noise to be extracted, Figure 1(e) shows the data after global lateral random reorder. Here, the flattened linear noise $\mathbf{S}_1$ remains linear, while the rest of the data turns into randomly distributed outlier noise. In the corresponding FK spectrum (Figure 1(f)), the energy of the linear noise is concentrated along the horizontal axis near zero wavenumber. We found that after global reorder, the energy concentration of the linear noise is significantly higher than in the rotation-flattened-only data, which enhances the sparsity of the linear noise in the transform domain and facilitates its extraction. In contrast, after multi-time-point lateral random reorder (Figures 1(g) and (h)), the energy of the discrete effective signal events becomes more scattered, while the energy of the target linear noise becomes more concentrated. This substantially improves the accuracy of linear noise extraction.

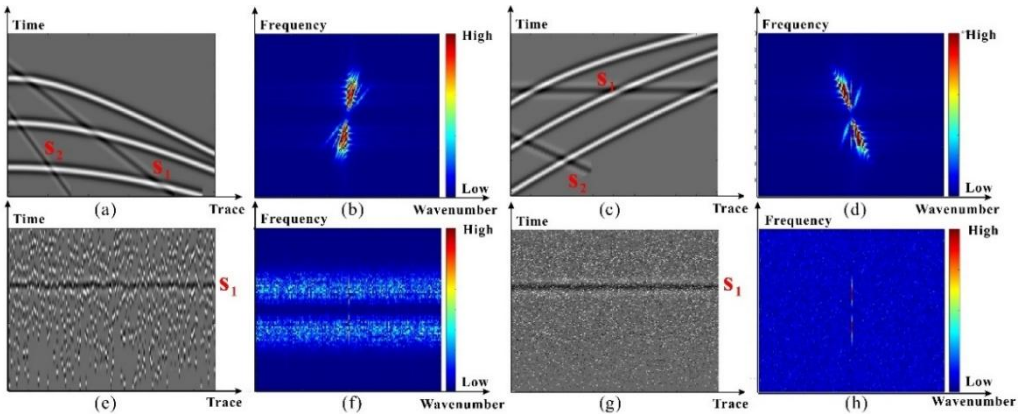


Fig. 1 Schematic illustration of lateral random reorder. (a) original data, (c) flattened linear events obtained using the rotating coordinate system, (e) result of (c) after global lateral random reorder, (g) result of (c) after multi-time-point lateral random reorder; (b), (d), (f), (h) FK spectra of (a), (c), (e), (g), respectively.

2. Linear noise suppression theory

After rotation-flattening and lateral random reorder, the effective signals are transformed into random outlier noise. We therefore employ the "Lp+Lp" framework for outlier noise attenuation to extract the linear noise. The data after rotation-flattening and lateral reorder can be expressed as $\mathcal{P}(\mathcal{L}(\mathbf{S}))$, and the corresponding optimization problem is formulated as follows:

$$J(\mathbf{S}_{linear}) = \min_{\mathbf{S}_{linear}} \|\mathbf{S} - \mathbf{S}_{linear}\|_p^p + \lambda \|\mathbf{B}\mathcal{P}(\mathcal{L}(\mathbf{S}_{linear}))\|_p^p \tag{7}$$

where $\mathbf{S}_{linear}$ denotes the linear noise to be extracted and $\mathbf{B}$ is the sparsity-promoting transform (the FK transform is adopted in this paper). After rotation-flattening, the apparent velocity of the linear noise becomes infinite and its wavenumber approaches zero. Based on the Alternating Direction Method of Multipliers (ADMM), the objective function is written as follows:

$$\begin{aligned} \underset{\mathbf{S}_{linear},\, \mathbf{Z},\mathbf{u}}{arg\min} \{J(\mathbf{S}_{linear},\, \mathbf{Z},\mathbf{u})\} = \underset{\mathbf{S}_{linear},\, \mathbf{Z},\mathbf{u}}{arg\min} & \|\mathbf{S} - \mathbf{S}_{linear}\|_p^p + \lambda_0 \|\mathbf{B}\mathcal{P}(\mathcal{L}(\mathbf{Z}))\|_p^p \\ & + \frac{\rho_0}{2} \|\mathbf{S}_{linear} - \mathbf{Z} + \mathbf{u}\|_2^2 \end{aligned} \tag{8}$$

Solving the above equation thus requires an alternating minimization over three variables, among which $\mathbf{X}^{true}$ can be updated as follows:

$$\mathbf{S}_{linear}^{(k+1)} = \underset{\mathbf{S}_{linear},\, \mathbf{Z},\mathbf{u}}{arg\min} \|\mathbf{S} - \mathbf{S}_{linear}^{(k)}\|_p^p + \frac{\rho_0}{2} \|\mathbf{S}_{linear}^{(k)} - \mathbf{Z}^{(k)} + \mathbf{u}^{(k)}\|_2^2 \tag{9}$$

The optimization problem in equation (9) can be solved using the Generalized Iterative Soft Thresholding algorithm:

$$\mathbf{S}_{linear}^{(k+1)} = \mathbf{S} - \mathrm{T}_{(1/\rho_0, p)}(\mathbf{S} - \mathbf{Z}^{(k)} + \mathbf{u}^{(k)}) \tag{10}$$

where $\mathrm{T}_{(\lambda,\, p)} = \max\{|x| - \lambda^{2-p}|x|^{p-1}\}\mathrm{sgn}(x)$, and variable $\mathbf{Z}$ can be updated as follows:

$$\mathbf{Z}^{(k+1)} = \lambda_0 \|\mathbf{B}\mathcal{P}(\mathcal{L}(\mathbf{Z}^{(k)}))\|_p^p + \frac{\rho_0}{2} \|\mathbf{S}_{linear}^{(k+1)} - \mathbf{Z}^{(k)} + \mathbf{u}^{(k)}\|_2^2 \tag{11}$$

The optimization problem in equation (11) can be solved using shaping regularization:

$$\mathbf{Z}^{(k+1)} = \mathcal{L}^{-1}\left(\mathcal{P}^{-1}\left(\mathbf{B}^{-1}\mathrm{T}_{(\lambda_0/\rho_0, p)}\mathbf{B}\mathcal{P}\left(\mathcal{L}\left(\mathbf{S}_{linear}^{(k+1)} + \mathbf{u}^{(k)}\right)\right)\right)\right) \tag{12}$$

Finally, the dual variable $\mathbf{u}$ is updated via the dual ascent method, with the

corresponding iterative update equation given by:

$$\mathbf{u}^{(k+1)} = \mathbf{u}^{(k)} + \mathbf{S}_{linear}^{(k+1)} - \mathbf{Z}^{(k+1)} \tag{13}$$

In summary, alternately iterating over the coupled equations (10), (12), and (13) yields the rotation-reorder-based linear noise extraction under the "Lp+Lp" framework (We set p=0.65 in this paper). The noise-free signal is finally obtained by inverse-flattening the extracted linear noise and subtracting it from the original seismic data.

Algorithm 1 summarizes the complete workflow of linear noise attenuation based on the rotation-flattening and lateral reorder operators, with the apparent velocity v_a of the linear noise supplied as a known input. In practice, the iterative loop usually converges well before the maximum iteration count $k_{\max}$ is reached. The regularization parameter, which is critical to the attenuation performance, is generally set to about 0.1 times the maximum amplitude of the "outlier noise" in the FK domain.

Algorithm 1: Linear Noise Suppression Based on ADMM ("Lp+Lp" Framework)

Input: $\mathbf{S}_0$, v_a

Select $\{\mathbf{S}(x,y) | \mathbf{S} \in \mathbb{R}^{m\times n}, m \leqslant m_0, n \leqslant n_0\}$ from $\mathbf{S}_0$ containing linear noise;

Calculate the dip of the linear event based on $\theta = \arctan(1/v_a)$;

Set parameters: maximum iteration number $k_{\max}$, regularization parameter λ_0, iteration step ρ_0;

Initialization parameters: $\mathbf{S}_{linear} = \mathbf{0}$, $k = 1$, iteration error eps

while $k < k_{\max}$ do

Let $\mathbf{X}^{true(0)} = \mathbf{0}$, $\mathbf{Z}^{(0)} = \mathbf{0}$, $\mathbf{u}^{(0)} = \mathbf{0}$

$$\mathbf{X}^{true(k+1)} = \mathrm{T}_{(\lambda_0/\rho_0,p)}(\mathbf{Z}^{(k)} - \mathbf{u}^{(k)} - \mathbf{S}_{linear}^{(k)}) \tag{A-1}$$

$$\mathbf{Z}^{(k+1)} = \mathcal{L}^{-1}\left(\mathcal{P}^{-1}\left(\mathbf{B}^{-1}\mathrm{T}_{(\lambda_0/\rho_0,p)}\mathbf{B}\mathcal{P}\left(\mathcal{L}\left(\mathbf{S}_{linear}^{(k+1)} + \mathbf{u}^{(k)}\right)\right)\right)\right) \tag{A-2}$$

$$\mathbf{u}^{(k+1)} = \mathbf{u}^{(k)} + \mathbf{S}_{linear}^{(k+1)} - \mathbf{Z}^{(k+1)} \tag{A-3}$$

$$k = k + 1$$

If $\|\mathbf{S}_{linear}^{(k+1)} - \mathbf{S}_{linear}^{(k)}\|_2^2 < eps$

Break;

End

End While

Output: data $\mathbf{S} - \mathbf{S}_{linear}$ after linear noise suppression

Details of equation (A-2):

By rotating the coordinate system by angle θ for $\mathbf{S}_{linear}^{(k)}$, we obtain: $\mathbf{S}'^{(k)} = \mathcal{L}\left(\mathbf{S}_{linear}^{(k)}\right)$;

Set the random reorder index $i \leftrightarrow index$;

Apply $\mathcal{P}\left(\mathbf{S}_{j,i_j}^{\prime(k)}\right) \mapsto \mathbf{S}_{j,index_j}^{\prime(k)}$ to $\mathbf{S}'^{(k)}$ for lateral random reorder, we get: $\mathbf{S}''^{(k)} = \mathcal{P}\left(\mathcal{L}\left(\mathbf{S}_{linear}^{(k)}\right)\right)$;

Apply the FK transform to the data $\mathbf{S}''^{(k)}$ after rotation and lateral random rearrangement, yielding: $\mathbf{X} = \mathbf{B}\left(\mathcal{P}\left(\mathcal{L}\left(\mathbf{S}_{j,index_j}^{\prime(k)}\right)\right)\right)$;

Apply generalized soft-thresholding to each element of $\mathbf{X}$: $\mathrm{T}_{(\lambda,\, p)} = \max\left\{|x| - \lambda^{2-p}|x|^{p-1}\right\}\mathrm{sgn}(x)$;

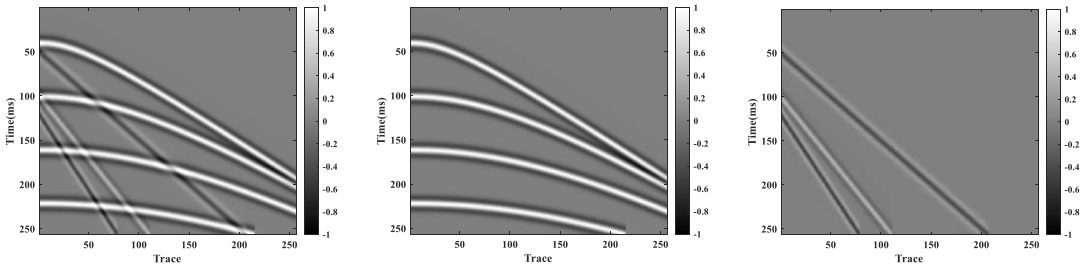
Apply the inverse FK transform followed by an inverse rotation with angle $-\theta$ to obtain: $\mathbf{S}_{linear}^{(k+1)} = \mathcal{L}^{-1}\left(\mathcal{P}^{-1}\left(\mathbf{B}^{-1}\mathrm{T}_{(\lambda,\, p)}\mathbf{X}\right)\right)$.

The overall workflow of the proposed method can be summarized as follows. First, a coordinate rotation is applied to orient all linear noise events horizontally. The traces are then randomly reordered along the lateral direction. After these two steps, the reflection events lose most of their lateral coherence in the rotated coordinate frame, whereas the linear noise remains continuous. Two reorder schemes can be distinguished. With the global lateral random reorder, a single permutation is applied to the entire dataset; the resulting truncation points along the signal waveforms cause spectral leakage, so that the reflections are split into discrete segments that behave like band-limited random outliers. With the multi-time-point lateral random reorder, an independent permutation is applied at each time sample, breaking the reflections down further into isolated, pulse-like outliers whose energy is distributed across the entire FK spectrum, while the energy of the flattened linear noise remains concentrated near zero wavenumber. Because the multi-time-point scheme makes the signal components more scattered and the target noise sparser in the transform domain, it improves the accuracy of linear noise extraction and is therefore adopted in all experiments in this paper. As long as the linear noise satisfies the stationarity assumption, its wavenumber energy remains concentrated near zero. The denoised output is finally obtained by isolating the sparsified linear noise component, applying the inverse FK transform, the inverse reorder, and the inverse rotation, and subtracting the resulting noise estimate from the input data. The key strength of the approach is that it considerably widens the gap between the linear noise and the remaining signals. For quasi-linear noise, the method can be adapted by first tracing the event paths in the T–X domain and approximating them with piecewise linear segments.

Applications

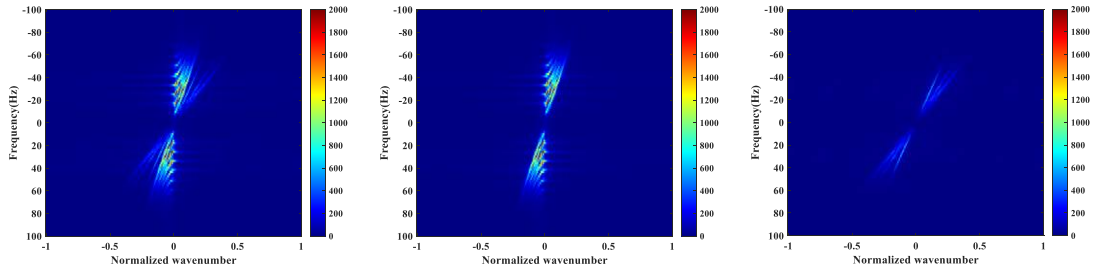
Synthetic Test 1

We first validated the proposed method on a simple synthetic model consisting of 256 traces with 256 time samples and a sampling interval of 1 ms. The noisy data in Figure 2(a) were obtained by summing the noise-free signal in Figure 2(b) and the synthetic linear noise in Figure 2(c). The three linear events have distinctly different dips from the effective signal, so conventional methods can also perform reasonably well on this example. Figure 3 shows the corresponding FK spectra, in which the dip contrast between the noise and the signal is clearly visible and the linear noise can be unambiguously recognized; such spectra are therefore used throughout the following tests for quality control (QC).



(a) (b) (c)

Fig. 2 Synthetic model 1. (a) noisy data, (b) original noise-free data, (c) synthetic linear noise.

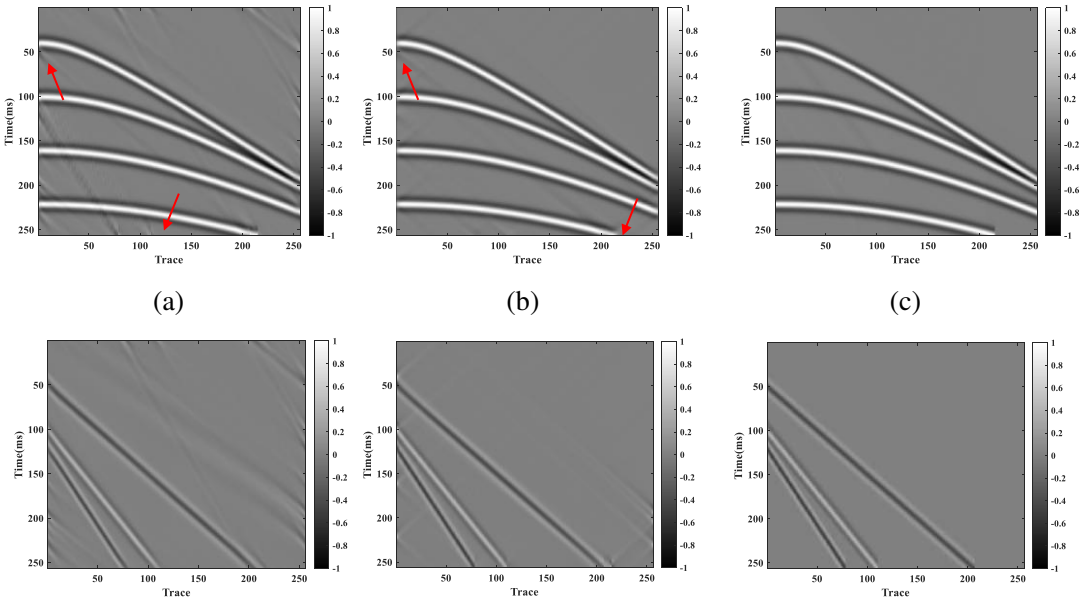


(a) (b) (c)

Fig. 3 FK spectra of (a) noisy data, (b) noise-free data, and (c) synthetic linear noise.

Three algorithms were compared: the FK transform, the Radon transform, and the proposed rotation-reorder-based method. All of them performed satisfactorily, removing most of the linear noise while largely keeping the energy of the desired signal. In the FK-filtered output (Figures 4(a) and 4(d)), abrupt zeroing of the noise components produced “FK truncation noise”, and the linear events at the edges (red arrows) were only partially removed. The Radon-based result (Figures 4(b) and 4(e)) still contains weak residual linear noise, caused by the overlap of noise and signal in the Radon domain (red arrows), together with truncation-induced artifacts. By contrast, the threshold-based strategy of the proposed method (Figures 4(c) and 4(f)) introduced

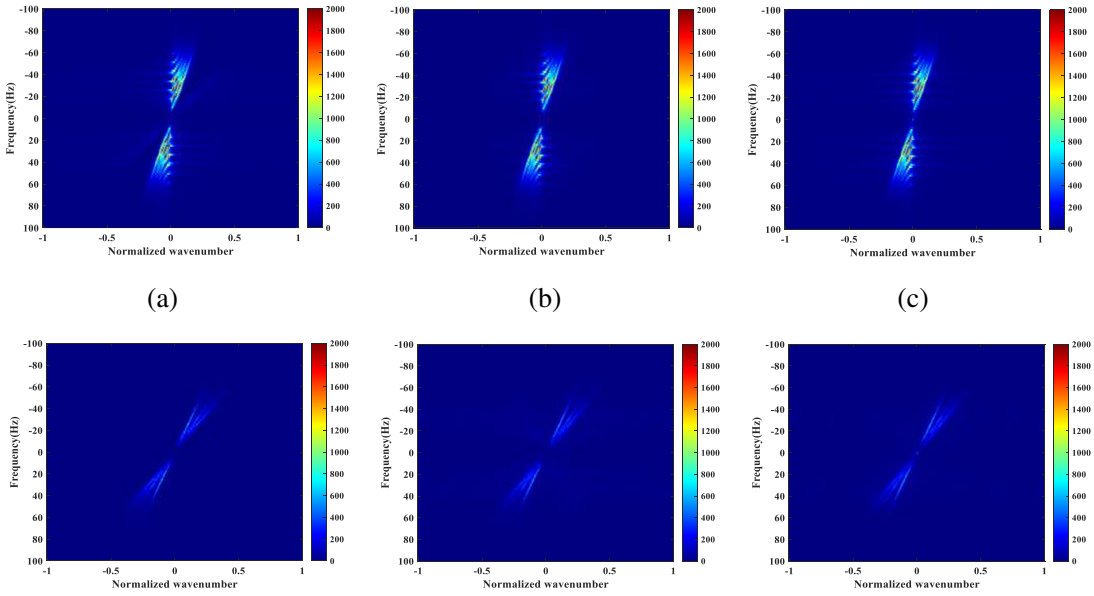
no extra noise and yielded the best overall performance, with no notable residual linear noise and no visible damage to the signal. Figure 5 shows the QC FK spectra of these outputs. In short, all three approaches work well on this simple model, and the extracted noise closely resembles the synthetic noise except for minor details. It should be noted, however, that the test is not demanding: the linear noise is strong and its apparent velocity clearly differs from that of the signal, the data contain only four signal events, and the noise covers the entire record across all traces and time samples.



(a) (b) (c)

(d) (e) (f)

Fig. 4 Linear noise attenuation results. Denoising result and removed linear noise using (a) and (d) FK filter, (b) and (e) Radon transform filter, (c) and (f) our method.



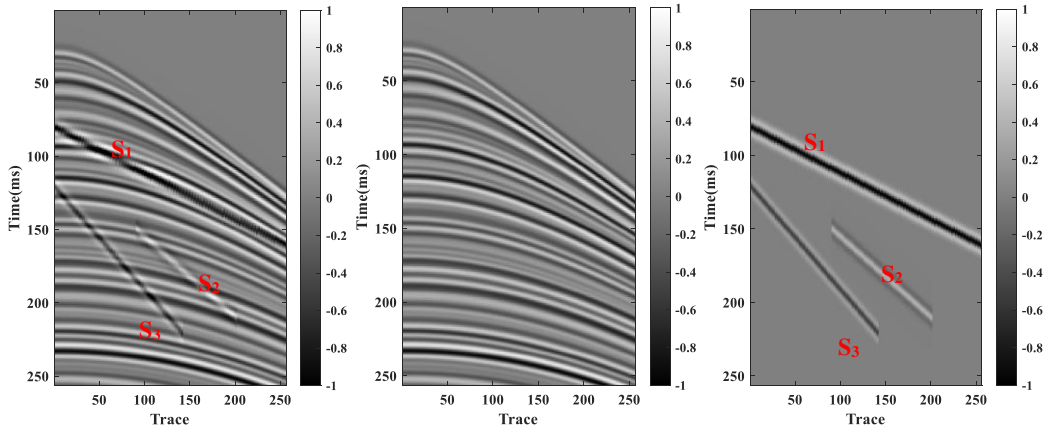
(a) (b) (c)

(d) (e) (f)

Fig. 5 FK spectra of denoising results and removed linear noise based on (a) and (d) FK filter, (b) and (e) Radon transform filter, (c) and (f) our method.

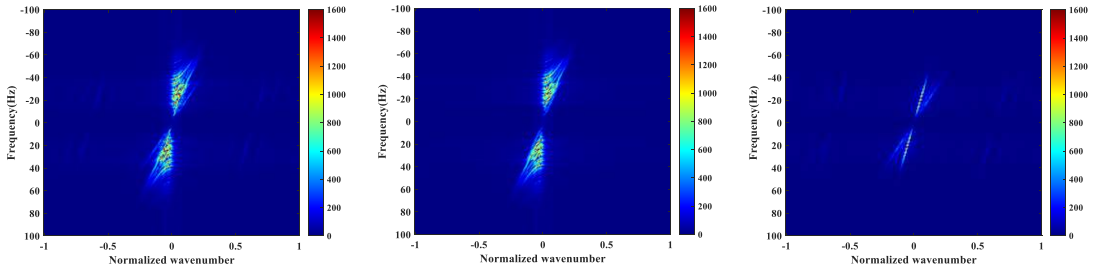
Synthetic Test 2

To examine the applicability of the method under more demanding conditions, we constructed a second, more complex synthetic model. Figure 6 shows the noisy data, the original noise-free data, and the synthetic linear noise. Here the reflection events are numerous and structurally intricate, so the data are far from sparse. Moreover, one noise component, S1, has a dip direction similar to that of the reflections, which greatly complicates noise suppression. Figure 7 displays the corresponding FK spectrum. Compared with Model 1, the spectral energy of the noise lies much closer to that of the signal; in particular, S1 overlaps almost completely with the signal energy in the FK domain, making this component virtually indistinguishable there.



(a) (b) (c)

Fig. 6 Synthetic model 2. (a) noisy data, (b) original noise-free data, (c) synthetic linear noise.



(a) (b) (c)

Fig. 7 FK spectra of (a) noisy data, (b) noise-free data, and (c) synthetic linear noise.

For comparison, FK filtering (Figures 8(a) and 8(d)) and Radon transform filtering (Figures 8(b) and 8(e)) were applied again. Both methods prove unable to suppress S1 effectively, since its dip closely resembles that of the signal; under such conditions, aggressive denoising inevitably harms the reflections. For the shorter noise segments S2 and S3, which do not extend over the entire trace length, both transforms also introduce edge effects. The proposed method (Figures 8(c) and 8(f)), in contrast, suppresses the noise more thoroughly while preserving the signal better, yielding a cleaner section. Nevertheless, a limitation was observed after flattening and reordering:

although the method greatly enlarges the noise – signal gap by making the signal more discrete and keeping the noise continuous, a small part of the signal energy whose dip resembles that of S1 can be drawn into the noise component in the FK domain. As a result, faint residual energy may appear around the extracted S1, though its amplitude is negligible and it is invisible in the final denoised result. Figure 9 shows the FK spectra of all outputs, confirming the effectiveness of the new method; the only discrepancy is a slight amplitude deviation in the extracted S1, which shares its direction with the signal.

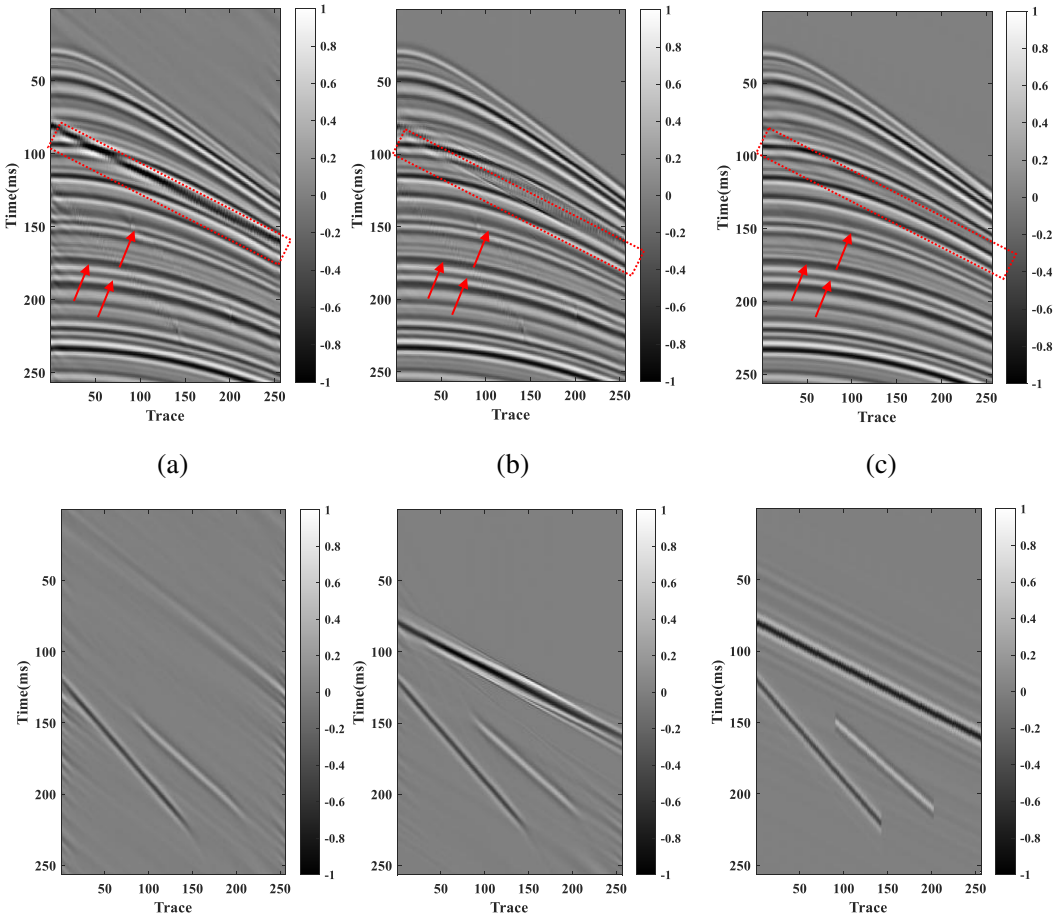
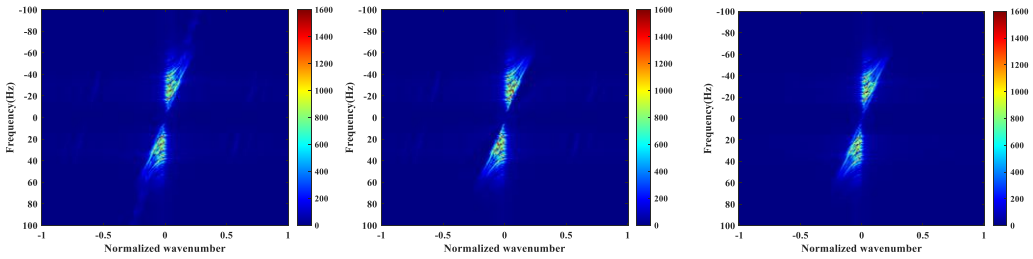
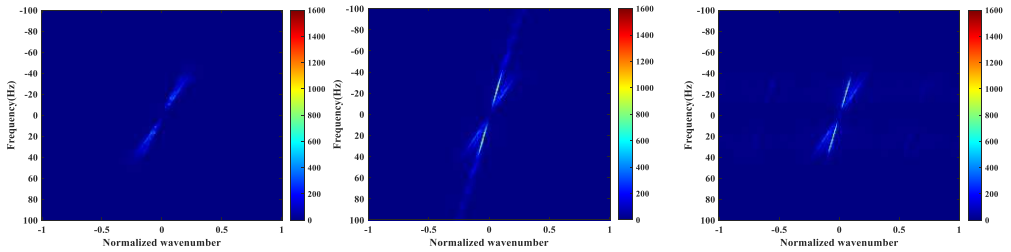


Fig. 8 Denoising result and removed linear noise using (a) and (d) FK filter, (b) and (e) Radon transform filter, (c) and (f) our method.





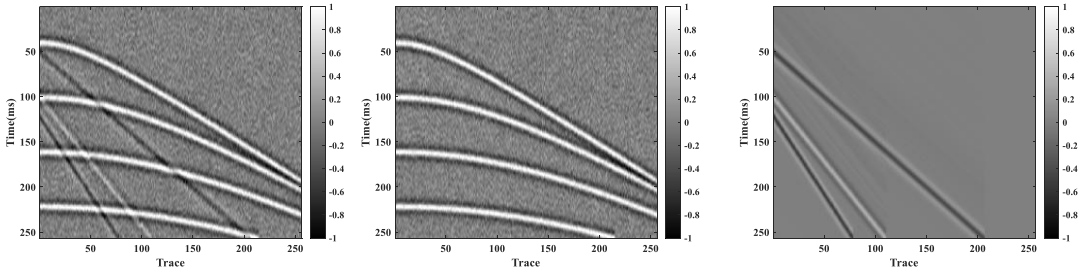
(d) (e) (f)

Fig. 9 FK spectra of (a) denoising result and (d) removed linear noise using FK filter, (b) denoising result and (e) removed linear noise using Radon transform filter, (c) denoising result and (f) removed linear noise using our method.

Noise Robustness Test

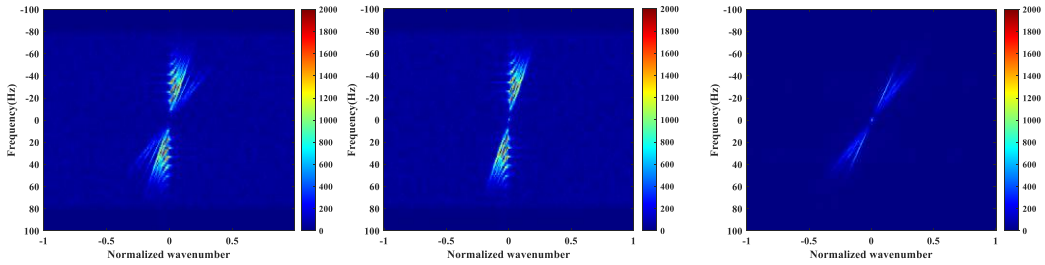
To assess robustness against random noise, we contaminated the Model 1 data with band-limited random noise whose maximum absolute amplitude reaches 0.5 times that of the signal. Figures 10(a) and 11(a) show the noisy profile (containing both linear and random noise) and its FK spectrum; the added noise shares the same upper frequency limit as the signal. Denoising with the proposed method yields the attenuation result in Figure 10(b) and the extracted noise in Figure 10(c), with a cosine similarity of 0.962 between the extracted and the original synthetic linear noise. The corresponding FK spectra are given in Figures 11(b) and 11(c). Satisfactory performance on this noisy dataset confirms both the signal-preservation capability and the noise robustness of the approach. Conceptually, the method works by thresholding in the FK domain: rotation and reordering leave the statistical characteristics of the random noise largely unchanged, so extracting the linear noise is equivalent to isolating the target linear noise from a mixture of random noise and “outliers” (the randomized reflections). Because the energy of the target noise remains concentrated, it can be reliably extracted.

For Model Test 2, the random noise level was raised so that the maximum absolute amplitude ratio between noise and signal reaches 0.85, again with identical upper frequency limits and a uniform spectral distribution within the band. Figures 12 and 13 show the noisy data, the denoising results, the extracted linear noise, and the FK spectra of these three datasets. The cosine similarity between the extracted and original synthetic linear noise is 0.976, and the method still performs favorably on this noisy, complex model. Under such strong background noise, the linear events are relatively weak and barely discernible in the FK spectrum, which severely limits FK filtering and Radon-domain filtering. The proposed method, by contrast, detects the linear noise from the original seismic data, builds a rotated coordinate system in the time – space domain, and only then applies thresholding in the FK domain.



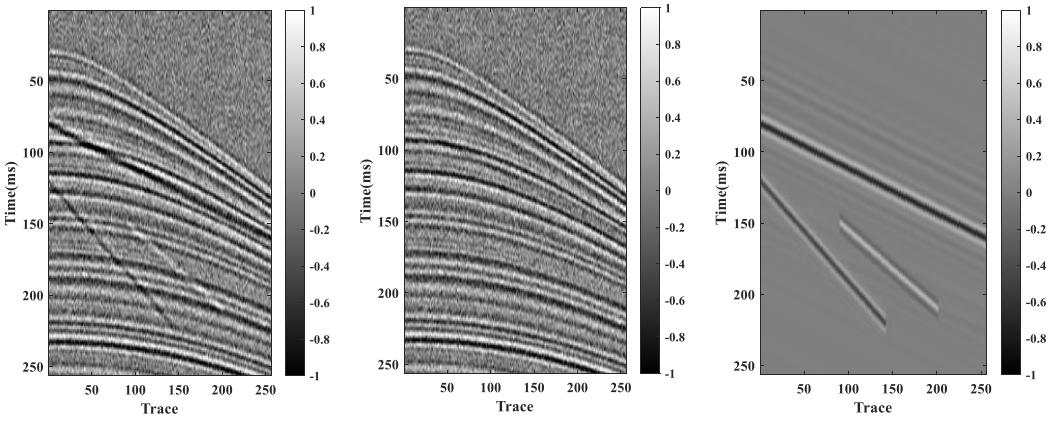
(a) (b) (c)

Fig. 10 Linear noise attenuation results. (a) synthetic model with random noise and linear noise, (b) denoising result and (c) removed linear noise using our method.



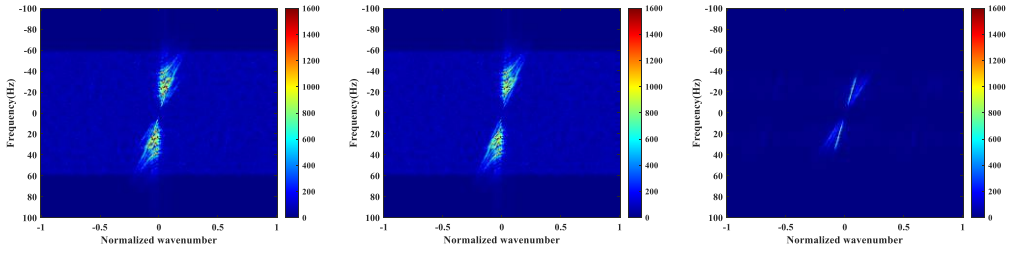
(a) (b) (c)

Fig. 11 FK spectra of (a) noisy synthetic model with random noise and linear noise, (b) denoising result and (c) removed linear noise using our method.



(a) (b) (c)

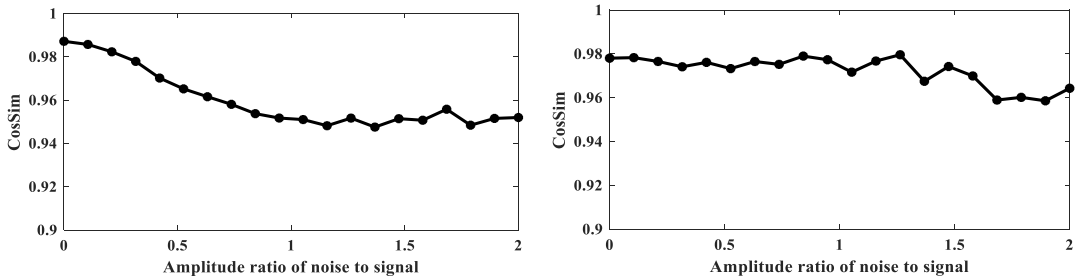
Fig. 12 Linear noise attenuation results. (a) synthetic model with random noise and linear noise, (b) denoising result, and (c) removed linear noise using our method.



(a) (b) (c)

Fig. 13 FK spectra of (a) noisy model with random noise and linear noise, (b) denoising result, and (c) removed linear noise using our method.

Figure 14 plots the cosine similarity between the extracted and original synthetic linear noise against the noise-to-signal amplitude ratio for the two synthetic tests. For both Model 1 and Model 2, the upper frequency limit and the spectral distribution of the random noise were kept fixed, and only the amplitude of the band-limited noise was increased step by step, with the horizontal axis representing the ratio of the maximum absolute amplitudes of noise and signal. Each configuration was repeated 10 times, and the averaged cosine similarity was taken as the final value. Over all tested noise levels, the similarity remained above 0.94 for both models, and the curves stayed stable as the noise amplitude grew, with the noise-to-signal maximum amplitude ratio varying from 0 to 2. These results confirm the strong noise robustness of the method.



(a) (b)

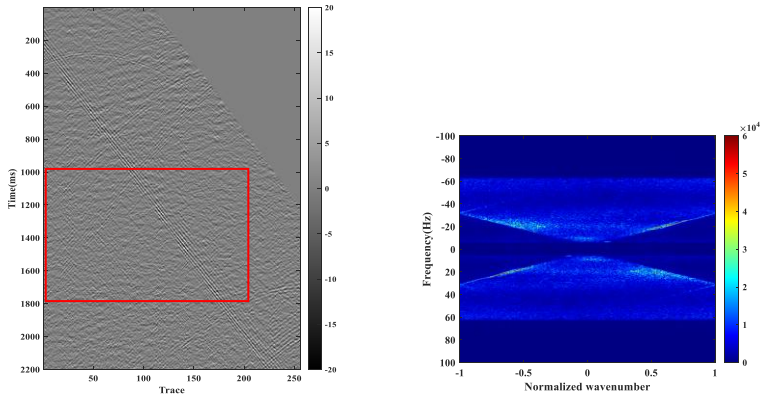
Fig. 14 Cosine similarity varying with noise-to-signal amplitude ratio of (a) Model 1, (b) Model 2.

Field data test

The method was further evaluated on a complete common-shot gather selected from a field dataset. As shown in Figure 15, the original profile and its FK spectrum contain strong linear interference that seriously degrades the imaging of deeper reflections. Linear noise attenuation was then performed with the FK filter (Figures 16(a) and 16(d)), the Radon-domain filter (Figures 16(b) and 16(e)), and the proposed rotation-reorder approach (Figures 16(c) and 16(f)). Both the FK filter and the proposed method removed the noise without visibly damaging the signal, whereas the Radon-domain filter impaired parts of the reflections because some noise events share similar dips with the signal. Overall, the proposed method suppressed the linear noise most effectively, yielding a cleaner profile and better imaging of the deeper section.

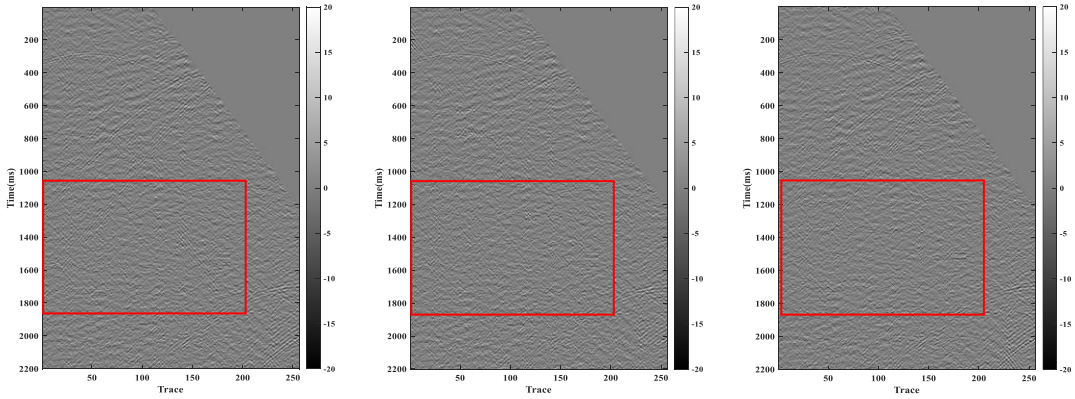
Figure 17 gives the FK spectra of the results in Figure 16. The FK-filtered output (Figures 17(a) and 17(d)) still retains some strong linear energy, and further aggressive suppression would risk damaging the signal. The Radon-domain filter (Figures 17(b) and 17(e)) eliminated the strong noise effectively, yet some weak linear components, which are hard to identify in the Radon domain, remain in the field data. The proposed method (Figures 17(c) and 17(f)) leaves the signal essentially intact while removing most of the strong linear energy. A zoomed-in view of a deeply buried zone with heavy

linear noise (Figure 18(a), 1000 – 1800 ms, traces 1 – 200) further illustrates this behavior: compared with the FK filter (Figure 18(b)) and the Radon filter (Figure 18(c)), the proposed method (Figure 18(d)) attenuates the strong noise more thoroughly with no obvious residual energy and handles the weaker noise arriving from various directions more effectively.

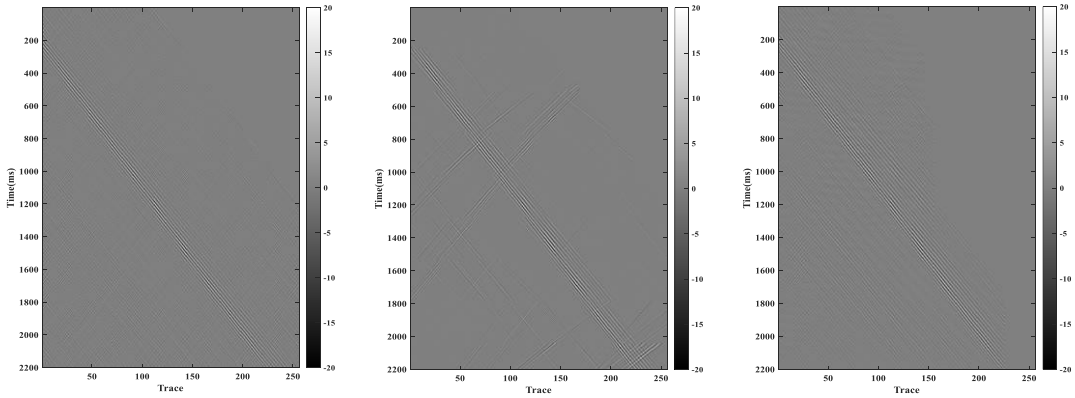


(a) (b)

Fig. 15 (a) original field data, (b) FK spectrum of (a).



(a) (b) (c)



(d) (e) (f)

Fig. 16 Linear noise attenuation results and removed linear noise using (a) and (d) FK filter, (b) and (e) Radon filter, (c) and (f) our method.

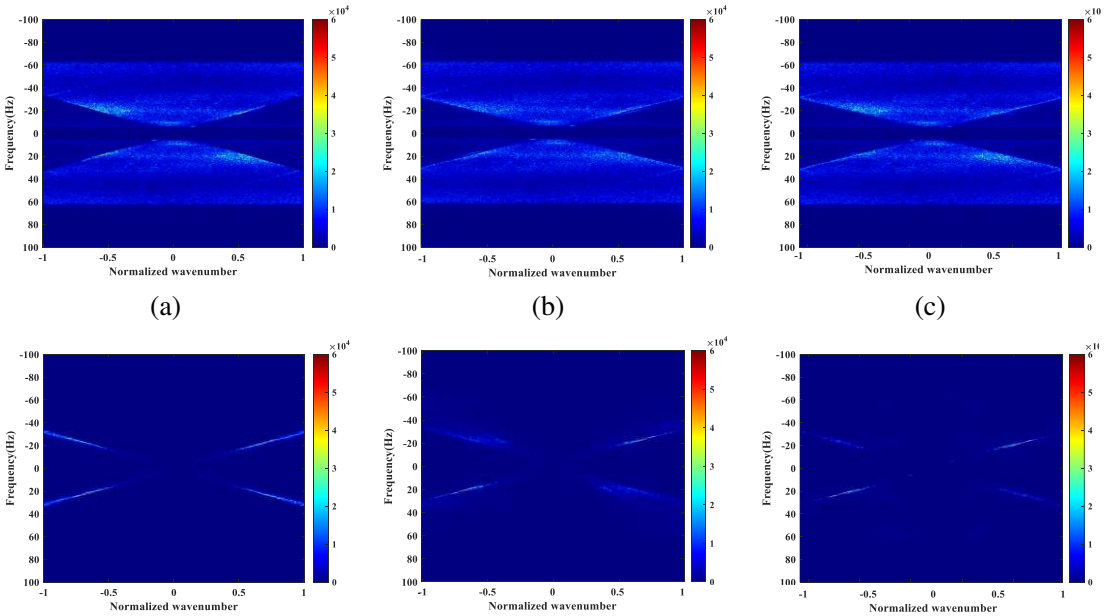


Fig. 17 FK spectra of denoising result and removed linear noise using (a) and (d) FK filter, (b) and (e) Radon filter, (c) and (f) our method.

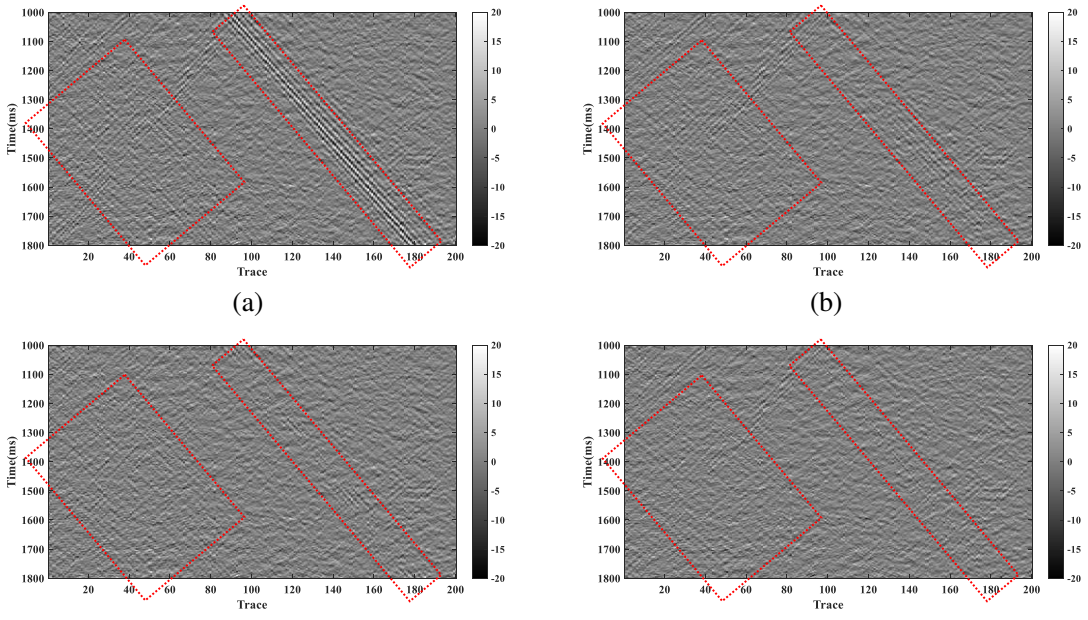


Fig. 18 Zoomed-in view of the region in the red box. (a) original data, (b) denoising result using the FK filter, (c) denoising result using the Radon filter, (d) denoising result using lateral random reorder.

Conclusions

In this paper, we have presented a framework for linear noise attenuation that combines coordinate rotation with lateral random permutation applied at each time sample to strengthen the sparsity of the linear noise. The pipeline turns coherent reflections into randomized, outlier-like components, thereby increasing the

separability between the primary reflections and the linear noise, so that noise extraction is recast as an outlier-suppression problem. An Lp-norm-based outlier attenuation algorithm (specifically, the "Lp+Lp" formulation) is then used to extract the noise component. For both synthetic models, the cosine similarity between the extracted and the true linear noise remained above 0.94 as the noise-to-signal amplitude ratio was increased from 0 to 2, and comparisons on a field common-shot gather showed that the proposed method suppresses linear noise effectively while preserving the signal. The main limitation of the method and possible extensions are discussed in the Discussions section.

Discussions

1. The proposed approach becomes less effective when the linear noise varies markedly over time in both frequency content and phase, a situation commonly observed in dispersive wave phenomena. As a remedy, future work will explore localized sliding windows oriented along the noise slope, combined with a localized random reordering strategy, to improve the suppression performance.

2. The current framework does not yet exploit the coherence of linear noise across adjacent profiles. Incorporating such information represents a promising direction for further methodological enhancement.

3. For noise events with strong spatial continuity, such as diffraction waves, a morphology-driven scheme can be designed to transform them into equivalent discrete outlier noise. Specifically, the events can be locally flattened and reordered along the estimated diffraction trajectories, under the assumption that diffractions within a sufficiently small local window can be well approximated as piecewise linear events.

Conflict of Interest

The authors declare no conflicts of interest regarding this work and hold no commercial or associative interests that could constitute a conflict in connection with the submitted manuscript.

Data Availability

The data that support the findings of this study are available from the corresponding author upon reasonable request.

Author Contribution Statement

All authors discussed the results, commented on the manuscript, and approved the final version.

References

Bekara M and Mirko V. Random and coherent noise attenuation by empirical mode decomposition [J]. Geophysics, 2009, 74(5): V89 – V98.

Chen S, Cao S, and Sun Y. Seismic linear noise attenuation based on the rotate-time-shift FK transform[J]. IEEE Geoscience and Remote Sensing Letters, 2021, 19: 1-5.

Gan Q G and Peng D J. Elimination of linear interference in time-space domain and its application[J]. Geophysical Prospecting for Petroleum (in Chinese), 2004, 43(2): 123-125, 129.

Gao S W, Zhao B, and Zhou X Y. Self-adaptive coherent noise attenuation technique[J]. Oil Geophysical Prospecting (in Chinese), 2003, 38(3): 242-246.

Henley D C. Coherent noise attenuation in the radial trace domain[J]. Geophysics, 2003, 68(4): 1408-1416.

Huang W, Wang R, Zhang D, et al. Mathematical morphological filtering for linear noise attenuation of seismic data[J]. Geophysics, 2017, 82(6): 369-384.

Liao J P, Wang H Z, Li W B, et al. 3D partial differential equation filtering and linear noise attenuation[J]. Geophysical Prospecting for Petroleum (in Chinese), 2007, 46(6): 550-556.

Liu G C, Chen X H, Li J Y, et al. Seismic noise attenuation using non-stationary polynomial fitting[J]. Applied Geophysics, 2011a, 8(1): 18-26.

Liu M Q, Yu X H, Zhou X L, et al. Coherent noise attenuation in broadside seismic data[J]. Geophysical Prospecting for Petroleum (in Chinese), 2011b, 50(3): 307-309, 318.

Lu E and Li Q C. The application of seismic noise attenuation based on hybrid radon transform[J]. Geophysical and Geochemical Exploration, 2013, 37(4): 706-710.

Lu W, Zhang W, and Liu D. Local linear coherent noise attenuation based on local polynomial approximation[J]. Geophysics, 2006a, 71(6): V163-V169.

Lu W. Adaptive noise attenuation of seismic images based on singular value decomposition and texture direction detection[J]. Journal of Geophysics and Engineering, 2006b, 3(1): 28-34.

Ö. Yilmaz. Seismic data analysis: processing, inversion, and interpretation of seismic data. Society of Exploration Geophysicists, 2001.

Tian Y C, Wang X W, Peng G X, et al. Noise attenuation technology on wide azimuth seismic data[J]. Oil Geophysical Prospecting (in Chinese), 2013, 48(2): 187-191.

Treitel S, Shanks J L, and Frasier C W. Some aspects of fan filtering[J]. Geophysics,

1967, 32(5): 789-800.
Turner G. Aliasing in the tau-p transform and the removal of spatially aliased coherent noise[J]. Geophysics, 1990, 55(11): 1496 – 1503.
Verschuur D J, Berkhout A J, and Wapenaar C P A. Adaptive surface-related multiple elimination[J]. Geophysics, 1992, 57(9): 1166-1177.
Wang Y. Multiple attenuation: coping with the spatial truncation effect in the Radon transform domain[J]. Geophysical Prospecting, 2003, 51(1): 75-87.
Yedlin M, Jones I, and Narod B. Applications of the Karhunen–Loève transform to diffraction separation[J]. IEEE Transactions on Acoustics, Speech, and Signal Processing, 1987, ASSP-35(1): 2-8.
Yuan Y, Zheng Y, and Si X. Attenuation of linear noise based on denoising convolutional neural network with asymmetric convolution blocks[J]. Exploration Geophysics, 2022, 53(5): 532-546.